Duration and decay of Arctic stratospheric vortex events in the ECMWF seasonal forecast model

Yvan J. Orsolini[1,3], Kazuaki Nishii[2], and Hisashi Nakamura[4]

[1] NILU - Norwegian Institute for Air Research, Kjeller, Norway

[2] Graduate School of Bioresources, Mie University, Mie, Japan

[3] Bjerknes Centre for Climate Research, Bergen, Norway

[4] Research Center for Advanced Science and Technology, University of Tokyo, Tokyo, Japan

submitted to Quart. J. Royal Meteorological Society, March 20, 2018; revised September 26, 2018

Corresponding author: Dr. Yvan J. ORSOLINI, NILU – Norwegian Institute for Air Research, N-2027 Kjeller, Norway (orsolini@nilu.no)

KEYWORDS : SEASONAL PREDICTION – STRATOSPHERE – POLAR – SEASONAL SCALE

ABSTRACT

Previous studies have documented extreme stratospheric polar vortex events, but the factors governing their duration have received little attention. Here, we investigate weak and strong stratospheric polar vortex events simulated in ensemble reforecasts for the Northern Hemisphere winter with the seasonal forecast model (System 4) of the European Centre for

Medium-Range Forecasting, in comparison with the European Reanalysis Interim dataset. The individual strong and weak vortex events are classified into short and long events. A composite analysis is conducted for each of the four categories of events with respect to their initial or end days. We examine the characteristics of each category in the forecast model and reanalyses, including anomalous zonal-mean zonal winds, heat and wave-activity fluxes, lower-tropospheric temperature and surface pressure, as well as the synoptic evolution of upper-tropospheric anomalies during the precursory and decaying stages.

The main findings are that (i) the forecast System 4 is found to produce both short and long anomalous vortex events in comparable amplitude to the reanalyses, but the polar zonal wind anomalies that are more persistent, for each of the four categories considered. (ii) Short events penetrate as deep as the long events right at their onset, but they rapidly decay under a wave forcing that is less sustained than in the long events. (iii) Subtle differences in the synoptic evolution of blocking Highs and Lows over both oceanic basins or over Northern Eurasia or America appear to condition the duration of the forcing. (iv) During such short events, characteristic surface or lower tropospheric signatures of the annular mode paradigm arising from the downward stratospheric influence are not allowed sufficient time to develop.

1. Introduction

The influence of the wintertime polar stratospheric variability on the tropospheric circulation and weather patterns at mid and high latitudes of the Northern Hemisphere has been well documented during the last two decades. There is ample evidence from both observations and model studies for the association between the planetary-wave driven sudden reversals of the polar night jet (known as stratospheric sudden warmings, SSWs) and tropospheric and surface circulation anomalies emerging within the weeks following their onset. These

tropospheric anomalies correspond to the negative phase of the Arctic Oscillation (AO), as a surface manifestation of the northern annular mode (NAM) extending downward from the stratosphere, with southward displacements of the jet stream and storm tracks both over the Atlantic and Pacific basins, and cold air outbreaks over Northern Eurasia and North America [e.g., Baldwin et al., 2003; Kolstad et al., 2010; Lethonen and Karpechko, 2016; Limpasuvan et al., 2004]. Episodes of stratospheric vortex intensification resulting from the weakening of planetary wave fluxes into the stratosphere are associated with largely opposing signatures [e.g., Limpasuvan et al., 2005; Orsolini et al., 2011; Dunn-Sigouin and Shaw, 2015].

The wintertime polar stratospheric variability is complex however, and there is a large event-to-event spread in vortex event duration. During SSWs for example, the duration of zonal-mean zonal wind reversals in the mid-stratosphere (typically at 10 hPa) can range from a few days to several weeks [e.g., Runde et al, 2016], and similarly, a strengthening of the vortex may be long- or short-lived. Moreover, a weakening of the vortex is not always accompanied by a reversal of zonal-mean westerly winds to easterlies. Adding to the complexity, there is some intra-seasonal variability in the characteristics of the events and their precursors [Diaz-Duran et al., 2017].

Nevertheless, little attention has been paid to the duration of these perturbed vortex events. Rather, much of the research focus has been placed on the apparent slow downward translation of stratospheric mean flow anomalies on the time scales of 1-2 months following SSWs, with a corresponding lagged surface impact. Composites of SSWs and strong vortex events in model simulations or reanalyses show that flow anomalies tend to form almost-simultaneously throughout the depth of the stratosphere after the onset of an event [Limpasuvan et al., 2004, 2005; Orsolini et al., 2011]. Using an idealised mechanistic model, Hitchcock and Haynes [2016] demonstrated how a deep, vertically synchronous suppression

of upward fluxes of wave activity is established within the stratosphere during the vortex recovery from SSWs.

Hence, there is a need for a better understanding of the factors controlling the duration of these perturbed vortex events, both in models and in the real atmosphere. The persistency of anomalous wave-activity flux emanating from the upper troposphere must be a key factor influencing the duration of those events [Polvani and Waugh, 2004]. Persistency of lower stratospheric anomalies around the onset of SSWs has also been shown to allow a tropospheric and surface NAM response [Karpechko et al., 2017; Maycock and Hitchcock 2015; Runde et al., 2016]. Details of the underlying dynamics are not clear, since the amplification of planetary wave fluxes occurs in the course of a coupled evolution of the stratosphere-troposphere system, through feedbacks between the mean state and the propagating waves. During that coupled evolution, the state of the stratosphere is as important as the anomalous wave activity flux emanating from the troposphere itself [Hitchcock and Haynes, 2016; Birner and Albers, 2017].

Stratospheric vortex events and their downward influence into the troposphere have been examined in reanalyses and in climate or chemistry-climate model simulations [e.g. Karpechko et al., 2017; Lethonen and Karpechko, 2016; Runde et al. 2016, and references therein]. However, relatively fewer studies have relied on operational monthly or seasonal dynamical prediction systems, which have higher resolution and different parametrisations [Maycock et al., 2011; Scaife et al., 2015; Tripathi et al., 2015b; Karpechko, 2018]. The above-mentioned findings, along with relatively long decorrelation time for the stratospheric NAM, suggest that enhancing stratospheric predictability on subseasonal-to-seasonal scales may yield benefit in extended prediction at the surface. Hence, considerable efforts have been undertaken to improve the prediction of SSWs with operational prediction systems, through a better representation of stratospheric mean state and variability, an increase in vertical

resolution in the model stratosphere and a raising of the model top to include the upper stratosphere and lower mesosphere. Although the deterministic predictability of SSW onset in such prediction systems is still limited to a lead time of 1-2 weeks, the predictability skill increases when initialised around the onset of SSWs or vortex intensification events [Sigmond et al, 2013; Tripathi et al., 2015b]. Hence, there is a forecast skill dependence on the stratospheric state [Scaife et al., 2015].

Besides actual predictability skill, it is yet unclear whether such forecast models realistically represent the full spectrum of observed events, from prolonged to short-lived ones, and their distinct characteristics in their stratospheric, tropospheric and surface signatures. The present paper makes an assessment of how the seasonal forecast model (System 4) of the European Centre for Medium-Range Forecasting (ECMWF) generically represents long and short vortex events, their near-surface impacts as well as their precursors. The System 4 had been the operational system until replaced by the new System 5 in November 2017. From a predictability viewpoint, it would be important to predict whether a particular vortex event under development is going to be long-lived or otherwise terminate rapidly, as it can potentially have different tropospheric and surface influences.

Assessing how the ECMWF seasonal forecast model reproduces the variety of durations of vortex events also requires an assessment of the model representation of the precursory intermittent tropospheric forcing and its interactions with the background (climatological) planetary waves. Such interactions modulate the total wave-activity flux into the stratosphere and ultimately, the polar vortex strength. Blocking Highs (BHs) play a crucial role in exerting this tropospheric forcing. They play, in fact, a dual role as the geographical location of BHs determines their stratospheric influence through their interaction with upper-tropospheric background planetary waves, adequately described in terms of quasi-linear interference [Orsolini et al., 2009; Woollings et al. 2010; Nishii et al., 2010; 2011; Dai and Tan, 2016;

Huang et al., 2017; Diaz-Duran et al., 2017]. BHs associated with the Western Pacific (WP) pattern were found to be precursors of strong vortex events, while BHs over the North Atlantic lead to long weak vortex events [Nishii et al., 2010, 2011; Dai and Tan, 2016].

2. Seasonal forecasts from the ECMWF System 4, and ancillary reanalysis data

We investigate stratospheric polar vortex events in the ECMWF System 4 (S4) coupled ocean-atmosphere seasonal prediction model of the ECMWF during the Northern Hemisphere winter. The performance and skill of an ensemble of state-of-the-art seasonal prediction systems, which comprise the high-top ECMWF S4, have been assessed by Butler et al. [2016], based on monthly-mean data. They showed that the magnitude and variability of the stratospheric polar night jet is well represented in S4, but also that such stratosphere-resolving high-top models do not have on average a higher seasonal prediction skill than their low-top counterparts, since the stratosphere is not predictable at a seasonal lead time as was previously stated [Maycock et al., 2011; Orsolini et al., 2011].

Forecasts with the ECMWF S4 system are also shown to predict the surface AO signal with high skill, although its magnitude is considerably smaller than in reanalyses [Stockdale et al., 2015]. It is not the aim of the present study to verify whether actual events are skilfully predicted in the ECMWF S4 system. Rather, we classify the simulated polar vortex events into short-lived and long-lived categories to differentiate their characteristics.

To this end, we use a series of 7-month forecasts over the period 1981-2014 with a start date on November 1. These forecasts are part of a set of S4 reforecasts extending to the year 2011, and operational forecasts are used afterwards. Among the 15-member ensemble reforecasts, we use a subset of 5 members for which the model level data for the upper stratosphere (above 10 hPa) was archived. As shown below, this 5-member ensemble for the 34-year period provides samples of polar vortex events with a variety of durations.

The atmospheric component of S4 is the Integrated Forecasting System (IFS) version 36r4, with horizontal resolution of T255 (approximately 80 km). The model has 91 levels extending up to 0.01 hPa, making it a high-top model. The daily reforecasts of horizontal wind velocities, temperature and geopotential height on 13 pressure levels in the stratosphere, ranging from 200 hPa to 1 hPa, as well as of sea level pressure (SLP) and 850-hPa temperature have been retrieved. All fields have been re-gridded onto a 2.5 latitude and longitude grid. The initial atmospheric conditions for the forecast were taken from the ECMWF ERA-Interim reanalyses (hereafter ERA-I). Through the initialisation, the quasi-biennial oscillation signature is introduced in the model, and likely sustained throughout the 7-month forecast period [Scaife et al., 2014]. After discarding the first month (November), we analyse the data for the period from December to March.

The duration of a given polar vortex event is determined on the basis of the NAM index, which is the principal component (PC1) of the first empirical orthogonal function of 10-hPa zonally-averaged geopotential height anomalies poleward of 20N, based on 8-day low-pass filtered anomalies from a daily model climatology. The climatology encompasses the 34 years and all the ensemble members. Weak (strong) vortex events, hereafter WVEs (SVEs), are defined as periods in which negative (positive) PC1 values in excess of a unit standard deviation persist over at least 5 days. The events with durations of 5~9 days are regarded as short events whereas those with durations of 20~29 days are regarded as long events. Our classification partially follows that of Tomikawa [2010], who examined the duration of the westward regime during SSWs in the Japanese 25-year reanalysis dataset, distinguishing short (less than 10 days, the typical radiative time scale at 10 hPa) and long (more than 20 days) events. The calculation of the autocorrelation of the model NAM index provides a decorrelation time (measured as the e-folding time scale) of 24 days. Thus, with the choice of a cut-off at 20 days, long events should represent vortex events with typical time scale of

stratospheric variability, while short events are much shorter-lived than this typical time scale. Note that extremely short events (with duration shorter than 5 days) are not considered.

In this manner, 21 (35) short WVEs (SVEs) and 25 (12) long WVEs (SVEs) have been identified, occurring in January-February. Events occurring in December or March were not retained in order to build long lag composites. Note that we do not attempt to distinguish between vortex splits and displacements, given the limited size of our ensemble of events. In a long climate model simulation, Maycock and Hitchcock [2015] found no differences in the surface signatures that were robust to the criteria used for classifying events and, for a given method of defining splits and displacements, the model data only showed small statistically robust differences. For each of the four categories, compositing is performed with respect to either the initial or the end day (the first or last day when the PC1 meets the above-mentioned criterion). While most of the previous studies composited vortex events according to their initial days, it is also instructive to construct composites with respect to the ending days of the events in featuring their decay processes. We examine key characteristics of each category in the forecast model at mid and high latitudes, such as the anomalous winds, temperatures, zonally-averaged Eliassen-Palm (E-P) flux and three-dimensional wave activity flux [Takaya and Nakamura, 2001].

To benchmark the results obtained with the forecast model, a similar composite analysis is carried out using ERA-I [Dee et al., 2011] over the period 1979-2016. The reanalysis data was retrieved on a 1.25°x1.25° latitude-longitude grid on 37 pressure levels from 1000 to 1 hPa. The numbers of selected events from ERA-I in the period of November to March consist of 16 (11) short WVEs (SVEs) and 20 (14) long WVEs (SVEs). The numbers of composited events across the 5-member ensemble in the forecast model are similar to those in ERA-I over a similar span of over three decades. One exception is the case of short SVEs, which are three times more in S4 with a member-wise distribution of 3, 9, 3, 10, 10 events, compared to

11 in the reanalyses. We stress again that we are investigating the generic characteristics of events, but not their frequency of occurrence, which is seemingly low-biased, as was noted before for SSWs [Maycock et al., 2011]. The date of events in ERA-I may not correspond to the simulated events in the long 7-month forecasts.

3. Analysis of long and short WVEs and SVEs in System 4 and in ERA-I.

3.1. Zonal-mean zonal winds, meridional heat and E-P fluxes

Figure 1 shows pressure-time cross-sections of the zonal-mean zonal wind anomalies and of the vertical component (EPz) and divergence of the E-P flux (EPFD) with respect to the ending day, for each of the four categories of vortex events in S4, i.e., short/long WVEs and SVEs. All quantities are averaged between 50N and 70N. Figure 2 shows the same cross-sections but composited with respect to their initial days. Albeit these two figures may be fairly redundant, we present them in order to highlight more clearly several aspects of the development and decay of vortex events.

Similarity between the long and short events at onset is more clearly observed in Fig. 2a-d. For both short and long WVEs, the zonal wind changes (Fig. 2a-d) are initiated in the upper stratosphere and then extend from 1 hPa down to 200 hPa at onset. Interestingly, zonal wind anomalies around the onset time for either WVEs or SVEs are nearly identical for short and long events, and they start to diverge in the days following the onset. For the long events, the zonal wind anomalies are hence not stronger initially, but they keep intensifying, from the upper stratosphere down to 200 hPa. While the evolution of zonal wind anomalies for the long WVEs and SVEs is fairly similar but mutually opposite (Fig.1b vs. Fig.1d), this is not quite the case for their short events. The short SVEs tend to occur following a period of persistent westerly anomalies associated with a moderately strong polar vortex. Compared to

the westerly anomalies within the short SVEs, the easterly anomalies within the short WVEs tend to develop more rapidly, become substantially stronger, and then decay more gradually.

Irrespective of their duration, WVEs (SVEs) tend to accompany enhancement (suppression) of upward wave-activity flux (EPz) in their development (Fig. 2e-h), followed by its suppression (enhancement) during their decay (Fig. 1e-h). Obviously, long WVEs tend to be accompanied by more persistent enhancement and suppression phases of EPz than short WVEs. It hence appears that the event duration and the persistency of the lower stratospheric wave forcing are closely tied, although both could be the manifestation of the same phenomenon in the coupled stratosphere-troposphere system [Birner and Albers, 2017]. The EPFD (Fig. 1i-l) for each of the categories is overall consistent with the corresponding time tendencies in zonal wind anomalies; i.e., the decay of WVEs (SVEs) accompanies an anomalous E-P flux divergence (convergence) that accelerates (decelerates) anomalous zonal-mean westerlies.

Turning now to ERA-I, Fig. 3 is the counterpart of Fig. 1, while Fig. 4 compares the 10-hPa zonal-mean zonal wind composite anomalies between the S4 and the reanalyses for each category. The compositing is made with respect to the end day. Figure 4 in particular reveals a greater persistence of weak zonal wind anomalies in S4 than in the re-analyses in all four categories. In short, the ending of either long or short events is less abrupt in S4 than in the reanalyses.

Figure 5 shows time series of zonal-mean anomalous meridional eddy heat flux (which is proportional to EPz), at 100 hPa and averaged between 45N and 90N, and its decomposition into a linear interference term (i.e., as the sum of covariance between climatological meridional winds and anomalous temperatures, and covariance between anomalous meridional winds and climatological temperatures) and a non-linear term (i.e., covariance

between anomalous meridional winds and anomalous temperatures), as in Nishii et al. [2010]. The anomalous heat flux and its decomposed contributions are based on composites for WVEs and SVEs relative to their initial days, averaged zonally and poleward of 45N. Short WVEs (SVEs) accompany of positive (negative) heat flux anomalies that are less persistent compared to long WVEs (SVEs), followed by a sign reversal of those anomalies a few days after onset, which should dynamically accelerate the recovery of stratospheric circulation anomalies. For both short and long WVEs (Fig. 5a-b), the linear and non-linear terms contribute comparably to the peak enhancement of the poleward heat flux. For SVEs, in contrast, the linear interference term dominates in the heat flux reduction, especially for long SVEs, which indicates the importance of the interaction of anomalies with the background planetary waves for SVEs [Nishii et al., 2011].

3.2 Synoptic evolution in the upper-troposphere

The importance of this interaction entices examination of geographical precursory and termination patterns in the upper troposphere, which may reveal why the meridional heat fluxes grow or decay. Figure 6 shows the correlation maps between the local 200-hPa geopotential height anomaly and the anomalous zonal-mean meridional eddy heat flux, at 100 hPa and averaged between 45N and 90N for a lag of -2 days, using all available days. In line with Nishii et al. [2011], they demonstrate contrasting tendencies for anticyclonic anomalies in the Asian/Pacific sector (blue shading) and the Euro-Atlantic sector (yellow shading) to reduce and enhance the heat flux, respectively, and vice versa for cyclonic anomalies. These tendencies are evident in the both ERA-I and S4. Whether blocking highs or lows move and develop in these respective sectors will condition the heat flux (i.e., upward wave-activity flux) and hence the polar stratosphere evolution. First and second columns of Fig. 7 (a-e-i, and b-f-j respectively) shows maps of 7-day averaged 200-hPa height anomalies in the course of the composited life-cycles of short and long WVEs, centred approximately 4 days prior to

and 4 days after the initial days of those events. More precisely, the averages correspond to days [-7, -1], days [-4, 2] and days [0, 6]. The maps are based on compositing with respect to the initial days given the particular emphasis here on precursory anomalies. Anomalous upward and downward components of wave-activity flux at 100-hPa are indicated by purple and green contours, respectively. If averaged zonally, this flux is equivalent to the E-P flux. Red arrows indicate the 200-hPa horizontal wave-activity flux defined by Takaya and Nakamura [2001], which represents horizontal wave-train propagation. Both long and short WVEs are characterised by a precursory zonal dipole consisting of an anomalous high over Scandinavia and an anomalous low farther to the east over Eastern Siberia, where a prominent planetary-wave trough is situated climatologically. In long events, the former high is stronger than in short events, and it further amplifies in the following 7-day period, slightly migrating westwards while maintaining a strong upward wave activity flux. Later, the anomalous high becomes pan-Arctic and thus more characteristic of a NAM signature. By contrast, in short events, the anomalous high over Scandinavia diminishes rapidly, and thus cannot sustain an upward wave activity flux. At the same time, a wave-train appears to emanate from the anomalous low over Eastern Siberia forming an anomalous high over Alaska (Fig. 7e), and then the high slowly retrogresses and approaches the climatological planetary-wave trough to contribute to rapid reduction of the upward wave-activity flux (Fig. 7i), as indicated by Nishii et al. [2011].

As shown in the rightmost column of Fig. 7d-h-l, long SVEs are characterised by a precursory anomalous high over the Gulf of Alaska and an anomalous low centred over the Hudson Bay. These tropospheric anomalies tend to persist during long SVEs, and the anomalous low intensifies even in the decay stage. The short SVEs (Fig. 7c-g-k) are also characterised by a precursory anomalous low over the Hudson Bay. However, it does not amplify, making a notable contrast to the long SVEs. The short events are also characterised

by an anomalous high over eastern Siberia (Fig. 7g), which rapidly evolves westward into a BH over Scandinavia within the fast termination of the events. In fact, a BH over Scandinavia is a characteristic precursor of WVEs, with augmented upward wave-activity flux as seen in Fig. 7b. During the rapid decay of the short SVE events (Fig. 7k), the upward wave-activity flux, which has been suppressed, increases to its climatological magnitude (Fig. 2e-f).

In summary, subtle differences in the evolution of upper-tropospheric anomalies over the North Atlantic, Northern Eurasia or the Western Pacific, appear to be related to the duration of the SVEs and WVEs. With respect to the corresponding composites based on the re-analysis data (Fig. 8), we first remark that the evolution of short events is dissimilar to its S4 counterpart, except the anticyclonic anomaly over Northern Europe. This could be a consequence of the large event-to-event variability for the case of short events, and of the relatively short sample size. By contrast, the evolution of long events share many common features between the S4 and reanalysis, such as the precursory Scandinavian blocking in long WVEs (Fig. 8b-f) or the persistent anomalous low over the Hudson Bay in long SVEs (Fig. 8d-h-l). During the evolution of long SVEs, there are nevertheless some differences in the North Pacific BH anomaly, which exhibits a more distinct retrogression from the Pacific to Eastern Siberia in the reanalyses (Fig. 8d-h-l) than in the S4 model (Fig. 7d-h-l).

3.3 Synoptic evolution in the lower troposphere and near the surface

The corresponding tropospheric and surface anomalies also differ between the short and long events. Figures 9 and 10 shows composited anomalies in SLP and 850-hPa temperature for S4 and the reanalyses, respectively, averaged over a two-week period following the end day, for each of the four categories of events. In their ending phase, both long events in S4 show prolonged polar and mid-latitude SLP anomalies similar to NAM signature but with opposing polarities between WVEs and SVEs (Fig. 9b and 9d, respectively), while in the reanalyses

these signatures are less pronounced (Fig. 10b and 10d). Note that the two-week averaging period is shorter than usually considered when looking at tropospheric impacts of, e.g., SSWs. Again, the evolution of short events is not necessarily similar between the S4 and ERA-I (Figs. 9a and 9c vs. Figs. 10a and 10c, respectively).

The temperature anomalies for long WVEs (Figs. 9f and 10f) are overall consistent with previous studies with respect to cold air outbreaks over Northern Eurasia and North America following SSWs [Kolstad et al., 2010; Lethonen and Karpechko, 2016]. Meanwhile, it is apparent that the short events tend to terminate before the characteristic NAM signatures emerge in lower-tropospheric temperature. For example, short WVEs in S4 are associated with warm temperature anomalies over Canada and Alaska (Fig. 9e), related to the wave-train emanating from eastern Siberia toward Alaska, and are hence opposite to the characteristic anomalies associated to the negative NAM in long WVE (Fig. 9f).

4. Discussion and Summary.

The ECMWF seasonal forecast system S4 produces both short and long stratospheric vortex events characterised by anomalies in comparable amplitude as in ERA-I, in terms of zonal-mean zonal wind, upper-tropospheric geopotential height, lower tropospheric temperatures or SLP. Nevertheless, polar zonal wind anomalies associated with the stratospheric polar-night jet tend to be more persistent than in ERA-I (e.g., Fig. 4), for each of the four categories considered, i.e., strong and weak events, long and short. Similarly, over-persistence of long SSWs compared to ECMWF ERA-40 re-analyses has been noted by Maycock and Hitchcock [2015] in a 1000-year climate model simulation. A first interpretation may be that the radiative damping time scale in the stratosphere is too long in the forecast model. However, in light of recent studies based on finite-amplitude wave interaction with the mean flow [Lubis et al., 2018; Martineau and Son, 2015], the over-persistence in the forecast model may

also arise from non-conservative wave damping processes that acts to delay the recovery of the vortex. The implication is that the unresolved, parametrised eddy mixing may be excessive and prolonged in the forecast model, retarding the recovery of the polar vortex.

Previous studies have classified long SSWs into events whose signatures are translating into the troposphere or not, with the former being less frequent. Our classification of WVEs and SVEs into short or long events nevertheless show that, in the composite of both long and short events, a high-latitude zonal-mean zonal wind anomaly that develops quasi-synchronously throughout the stratosphere down to at least 200 hPa (Figs. 1, 2). During short events, this anomaly peaks at the time of maximum zonal-mean zonal wind anomaly in the upper stratosphere (1hPa) before decaying rapidly (Fig. 1a-c), while it keeps amplifying throughout the stratosphere during long events. Hitchcock et al. [2013] pointed out that the duration of long SSWs events is correlated with the depth of their downward penetration, with a tendency for deeper events to be longer-lasting. Our analysis reveals that anomalies in the short events penetrate as deep as those in the long events right at their onset (Fig. 2). Afterwards, they rapidly decay under a wave forcing that is less sustained than during long events, which by contrast, continue to develop in strengthening zonal wind anomalies throughout the stratosphere (Fig. 1). The long and short events of the anomalous stratospheric polar vortex also show different evolutions of the lower-tropospheric and near-surface anomalies. During short events, the characteristic NAM paradigm signatures are not allowed sufficient time to develop.

In the days following the onset, the persistency of the forcing appears critical to determine the evolution of a polar vortex event into a short or long one, as was noted by Karpechko et al. [2017]. Subtle differences in the synoptic evolution of blocking highs and of anomalous lows over the two oceanic basins or over Northern Eurasia or North America appear to condition the duration of the events. For WVEs, persistent development of a Scandinavian BH tends to

lead to a long event, and associated anomalies will evolve into a characteristic NAM signature. For SVEs, by contrast, the persistence or decay of an anomalous low over the Hudson Bay is prompting the intensification of the polar vortex or its demise. The decay of short events subtly differs between S4 and the reanalyses. This synoptic evolution shown here based on ERA-I is nearly identical if based on the Japanese 55-year Reanalysis (JRA-55) dataset over the same period 1979-2016 (not shown), albeit with small differences in the selected list of short events. This gives us confidence in the robustness of the reanalysis composites for the observed period. Although it is a challenging issue to accurately reproduce such evolving blocking Highs or Low events in the coupled troposphere-lower stratosphere system, it appears that this evolution might need to be better captured in forecast models.

Acknowledgements. The authors are grateful for the two anonymous reviewers for their sound criticism and constructive comments. YOR was supported by the EU project SPECS funded by the European Commission's Seventh Framework Research Programme under the grant agreement 308378. KN and HN are supported in part by the Japanese Ministry of Education, Culture, Sports Science and Technology (MEXT) through the Arctic Challenge for Sustainability (ArCS) Program, the Japanese Ministry of Environment through the Environment Research and Technology Department Fund 2-1503, and the Japan Science and Technology Agency (JST) through Belmont Forum CRA "InterDec". The three authors also acknowledge the support from the Norwegian Research Council collaborative project between Japan and Norway (NORPAN #250135), and the help by Retish Senan (ECMWF) in handling the data.

References

Baldwin MP, Stephenson DB, Thompson DWJ, Dunkerton TJ, Charlton AJ, O' Neill A. 2003. Stratospheric memory and skill of extended-range weather forecasts. *Science*. **301**:636–640, doi:10.1126/ science.1087143.

Birner T, Albers JR. 2017. Sudden stratospheric warmings and anomalous upward wave activity flux, *SOLA*. **13A**:8-12.

Butler AH, Arribas A, Athanassiadou M, Baehr J, Calvo N, Charlton-Perez A, Déqué M, Domeisen DIV, Fröhlich K, Hendon H, Imada Y, Ishii M, Iza M, Karpechko AYu, Kumar A, MacLachlan C, Merryfield WJ, Müller WA, O'Neill A, Scaife AA, Scinocca J, Sigmond M, Stockdale TN, Yasuda T. 2016. The Climate-system Historical Forecast Project: do stratosphere-resolving models make better seasonal climate predictions in boreal winter?. *Q.J.R. Meteorol. Soc.*, **142**: 1413–1427. doi:10.1002/qj.2743

Dai Y, Tan B. 2016. The western Pacific pattern precursor of major stratospheric sudden warmings and the ENSO modulation. *Env. Res. Lett.*. **11**:124032, doi:10.1088/1748-9326/aa538a.

Dee DP et al. 2011. The ERA–interim reanalysis: Configuration and performance of the data assimilation system. *Q. J. Roy. Meteor. Soc.*. **137**:553–597.

Diaz-Duran A et al. 2017. Intra-seasonal variability of extreme boreal stratospheric polar vortex events and their precursors. *Clim. Dyn.*, **49**(9), DOI 10.1007/s00382-017-3524-1.

Dunn-Sigouin E, Shaw TA. 2015. Comparing and contrasting extreme stratospheric events, including their coupling to the tropospheric circulation. *J. Geophys. Res. Atmos.*, **120**:1374-1390, doi:10.1002/2014JD022116.

Hitchcock P, Shepherd TG, Manney GL. 2013. Statistical Characterization of Arctic Polar-Night Jet Oscillation Events. *J. Climate*. **26**:2096–2116

Hitchcock P, Haynes P. 2016. Stratospheric control of planetary waves. *Geophys. Res. Lett.*, **43***: 11884-11892*, doi:10.1002/2016GL071372.

Huang J, Tian W, Zhang J, Huang Q, Tian H, Luo J. 2017. The connection between extreme stratospheric polar vortex events and tropospheric blockings. *Q.J.R. Meteorol. Soc,* **143**: 1148–1164. doi:10.1002/qj.3001

Karpechko A Yu, Hitchcock P, Peters DHW, Schneidereit A. 2017. Predictability of downward propagation of major sudden stratospheric warmings. *Q.J.R. Meteorol. Soc.*, **143**: 1459–1470. doi:10.1002/qj.3017

Karpechko A Yu. 2018. Predictability of Sudden Stratospheric Warmings in the

ECMWF Extended-Range Forecast System, *Mon. Wea. Rev.*, **146**, 1063–1075.

Kolstad EW, T Breiteig, AA Scaife. 2010. The association between stratospheric weak polar vortex events and cold air outbreaks in the Northern Hemisphere. *Quart. J. Roy. Meteor. Soc.*, **136***:*886-893.

Lehtonen I, Karpechko AYu .2016. Observed and modeled tropospheric cold anomalies associated with sudden stratospheric warmings. *J. Geophys. Res. Atmos.*, **121**, 1591–1610, doi:10.1002/2015JD023860.

Limpasuvan V, Thompson DWJ, Hartmann DL. 2004. The life cycle of the Northern Hemisphere sudden stratospheric warmings. *J. Climate*, **17**:2584-2596.

Limpasuvan V, Hartmann DL, Thompson DWJ, Jeev K, Yung YL. 2005. Stratosphere-troposphere evolution during polar vortex intensification. *J. Geophys. Res.*, **110**:D24101, doi:10.1029/2005JD006302.

Lubis SW, Huang CS, Nakamura N, Omrani N, Jucker M. 2018. Role of Finite-Amplitude Rossby Waves and Nonconservative Processes in Downward Migration of Extratropical Flow Anomalies. *J. Atmos. Sci*., **75**, 1385–1401

Martineau P, Son S. 2015. Onset of Circulation Anomalies during Stratospheric Vortex Weakening Events: The Role of Planetary-Scale Waves. *J. Climate*, **28**, 7347–7370, https://doi.org/10.1175/JCLI-D-14-00478.1

Maycock AC, Keeley SPE, Charlton-Perez AJ, Doblas-Reyes FJ. 2011. Stratospheric circulation in seasonal forecasting models: implications for seasonal prediction. *Clim. Dyn.*, **36**:309, DOI: 10.1007/s00382-009-0665-x

Maycock AC, Hitchcock P. 2015. Do split and displacement sudden stratospheric warmings have different annular mode signatures?. *Geophys. Res. Lett.*, **42**: 10,943–10,951, doi:10.1002/2015GL066754.

Nishii K, Nakamura H, Orsolini YJ. 2010. Cooling of the wintertime Arctic stratosphere induced by the Western Pacific teleconnection pattern. *Geophys. Res. Lett.*. **37**:L13805, doi:10.1029/2010GL043551.

Nishii K, Nakamura H, Orsolini YJ. 2011. Geographical dependence observed in blocking high influence on the stratospheric variability through enhancement and suppression of upward planetary-wave propagation. *J. Climate*, **24**:6408–6423, doi:10.1175/JCLI-D-10-05021.1.

Orsolini YJ, Karpechko, AYu, Nikulin G. 2009. Variability of the Northern Hemisphere polar stratospheric cloud potential: the role of North Pacific disturbances. *Q.J.R. Meteorol. Soc.*, **135:** 1020–1029. doi:10.1002/qj.409

Orsolini YJ, Kindem IT, Kvamstø NG. 2011. On the potential impact of the stratosphere upon seasonal dynamical hindcasts of the North Atlantic Oscillation: a pilot study. Clim Dyn 36:579, doi:10.1007/s00382-009-0705-6

Polvani LM, Waugh DW. 2004. Upward wave activity flux as a precursor to extreme stratospheric events and subsequent anomalous surface weather regimes. *J. Climate*, **17**:3548-3554.

Runde T, Dameris M, Garny H, Kinnison DE. 2016. Classification of stratospheric extreme events according to their downward propagation to the troposphere. *Geophys. Res. Lett.*, **43**:6665–6672, doi:10.1002/2016GL069569.

Scaife AA et al. 2014. Predictability of the quasi-biennial oscillation and its northern winter teleconnection on seasonal to decadal timescales, *Geophys.Res. Lett*., **41**:1752–1758, doi:10.1002/2013GL059160.

Scaife AA, Karpechko AYu, Baldwin MP, Brookshaw A, Butler AH, Eade R, Gordon M, MacLachlan C, Martin N, Dunstone N, Smith D. 2016. Seasonal winter forecasts and the stratosphere. *Atmos. Sci. Lett.*, **17**: 51–56. doi:10.1002/asl.598

Sigmond M, Scinocca JF, Kharin VV, Shepherd TG. 2013. Enhanced seasonal forecast skill following stratospheric sudden warmings. *Nature Geoscience*, 6:98–102, doi:10.1038/ngeo1698.

Stockdale TN et al. 2015. Atmospheric initial conditions and the predictability of the Arctic Oscillation. *Geophys. Res. Lett.* **42***:*1173-1179, doi:10.1002/2014GL062681.

Takaya K, Nakamura H. 2001. A formulation of a phase independent wave-activity flux of stationary and migratory quasi-geostrophic eddies on a zonally varying basic flow. *J. Atmos. Sci.*, **58**:608–627.

Tomikawa Y. 2010. Persistence of easterly wind during major stratospheric sudden warmings. *J. Climate.* **23**:5258-5267.

Tripathi OP, Baldwin M, Charlton-Perez A, Charron M, Eckermann SD, Gerber E, Harrison RG, Jackson DR, Kim B-M, Kuroda Y, Lang A, Mahmood S, Mizuta R, Roff G, Sigmond M, Son S-W. 2015. The predictability of the extratropical stratosphere on monthly time-scales and its impact on the skill of tropospheric forecasts. *Quart. J. Roy. Meteor. Soc.*, **141**:987-1003.

Tripathi OP et al. 2015. Enhanced long-range forecast skill in boreal winter following stratospheric strong vortex conditions. *Env. Res. Lett.* **10**:104007.

Woollings T, Charlton-Perez AJ, Ineson S, Marshall AG, Masato G. 2010. Associations between stratospheric variability and tropospheric blocking. *J. Geophys. Res.*, **115**:D06108, doi:10.1029/2009JD012742.

CAPTIONS

Figure 1. Composite evolution of zonal-mean zonal winds, E-P fluxes in S4. Pressure/time cross-sections of zonal-mean zonal wind anomalies averaged between 50N and 70N, composited separately for (a) short WVEs, (b) long WVEs, (c) short SVEs and (d) long SVEs (contoured for every 5 m s^{-1}). Significant positive and negative anomalies at the 90% confidence level based on the t-statistic are indicated with yellow and light blue shading, respectively. Time axis is relative to the end day (day 0), as indicated by the vertical red line. (e-h) Same as in (a-d), respectively, but for anomalies of the vertical component of the E-P flux (EPz), multiplied by p/p_0 where p denotes pressure (hPa) and p_0 = 1000 hPa (contoured for every 3 kg m^{-1} s^{-2}) (i-l) Same as in (a-d), respectively, but for anomalous divergence of the E-P flux (EPFD) multiplied by p/p_0. (contoured for every 1 m s^{-2}). Horizontal red lines indicate the 10 hPa and 100 hPa levels.

Figure 2. As in Fig. 1, but with time axis is relative to the initial day (day 0), as indicated by the vertical red line.

Figure 3. **Composite evolution of zonal-mean zonal winds, E-P fluxes in ERA-I.** As in Fig. 1, but for composite maps based on ERA-Interim reanalysis data.

Figure 4. Composite evolution of 10-hPa zonal-mean zonal winds (a-d) Composites of zonally-averaged anomalies in 10-hPa zonal wind with respect to the end day for short SVE, long SVE, short VWE and long VWE in S4 (contoured for every 5 m s^{-1}). (bottom row) Same

as in (e-h), but for ERA-Interim reanalyses. Horizontal and vertical red lines indicate day 0 and 60N, respectively.

Figure 5. Time series of anomalous meridional eddy heat flux in S4. The fluxes at 100 hPa (black line: K m s^{-1}) are averaged zonally and poleward of 45N, and are based on composites constructed separately for the (a) short WVEs, (b) long WVEs, (c) short SVEs, and (d) long SVEs relative to their initial days (day 0; red dashed line). The blue and red lines represent the contributions from the quasi-linear and non-linear interaction terms, respectively, to the anomalous heat flux, with dots indicating 90% confidence level.

Figure 6. Correlation between 200-hPa height and 100-hPa meridional eddy heat flux anomalies in S4 and ERA-I.

The correlation map between the 200-hPa height anomalies and the 100-hPa anomalous meridional eddy heat flux, averaged zonally and poleward of 45N, at a lag of – 2 days for S4 (a) and ERA-I (b), using all available days. Significant positive and negative correlations at the 99% confidence level are indicated with yellow and light blue shading, respectively.

Figure 7. Composite of upper-tropospheric geopotential height anomalies in S4. Sequence of 200-hPa geopotential height composite maps (contoured for every 50 m, with solid being positive and dashed negative) for 6-day averaged periods through the life-cycle of short WVEs (first column, a-e-i), long WVEs (second column, b-f-j), short SVEs (third column, c-g-k), and long SVEs (forth column, d-h-l), centered on days [-7, -1], days [-4, 2], and days [0, 6], relative to the initial day. Significant positive and negative anomalies at the 90% confidence level are indicated with yellow and light blue shading, respectively. The purple (green) contours indicate positive (negative) 100-hPa anomalous vertical flux of wave activity (± 0.01 m^2/s^2), while red arrows indicate the 200-hPa horizontal flux of Takaya and Nakamura [2001] (m^2/s^2).

Figure 8. Composite of upper-tropospheric geopotential height anomalies in ERA-I. (As in Fig. 7).

Figure 9. Composited maps of SLP and 850-hPa temperature anomalies in S4. Maps of SLP (upper; contoured for every 2 hPa) and temperature (lower; contoured for every 1 K) composited for days [1,14] with respect to the end days for short WVEs (first column, a-e), long WVEs (second column, b-f), short SVEs (third column, c-g-), and long SVEs (forth column, d-h). Significant positive and negative anomalies at the 90% confidence level are indicated with yellow and light blue shading, respectively.

Figure 10. Composited maps of SLP and 850-hPa temperature anomalies anomalies in ERA-I. (As in Fig. 9)

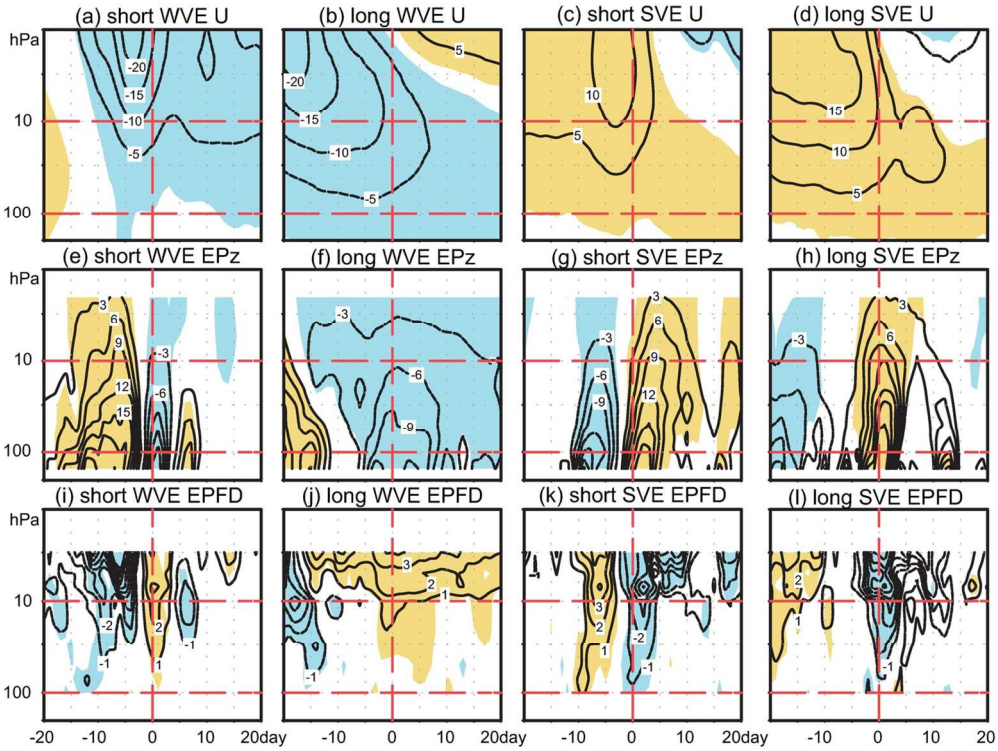

Figure 1. Composite evolution of zonal-mean zonal winds, E-P fluxes in S4. Pressure/time cross-sections of zonal-mean zonal wind anomalies averaged between 50N and 70N, composited separately for (a) short WVEs, (b) long WVEs, (c) short SVEs and (d) long SVEs (contoured for every 5 m s^{-1}). Significant positive and negative anomalies at the 90% confidence level based on the t-statistic are indicated with yellow and light blue shading, respectively. Time axis is relative to the end day (day 0), as indicated by the vertical red line. (e-h) Same as in (a-d), respectively, but for anomalies of the vertical component of the E-P flux (EPz), multiplied by p/p0 where p denotes pressure (hPa) and p0 = 1000 hPa (contoured for every 3 kg m^{-1} s^{-2}) (i-l) Same as in (a-d), respectively, but for anomalous divergence of the E-P flux (EPFD) multiplied by p/p0. (contoured for every 1 m s^{-2}). Horizontal red lines indicate the 10 hPa and 100 hPa levels.

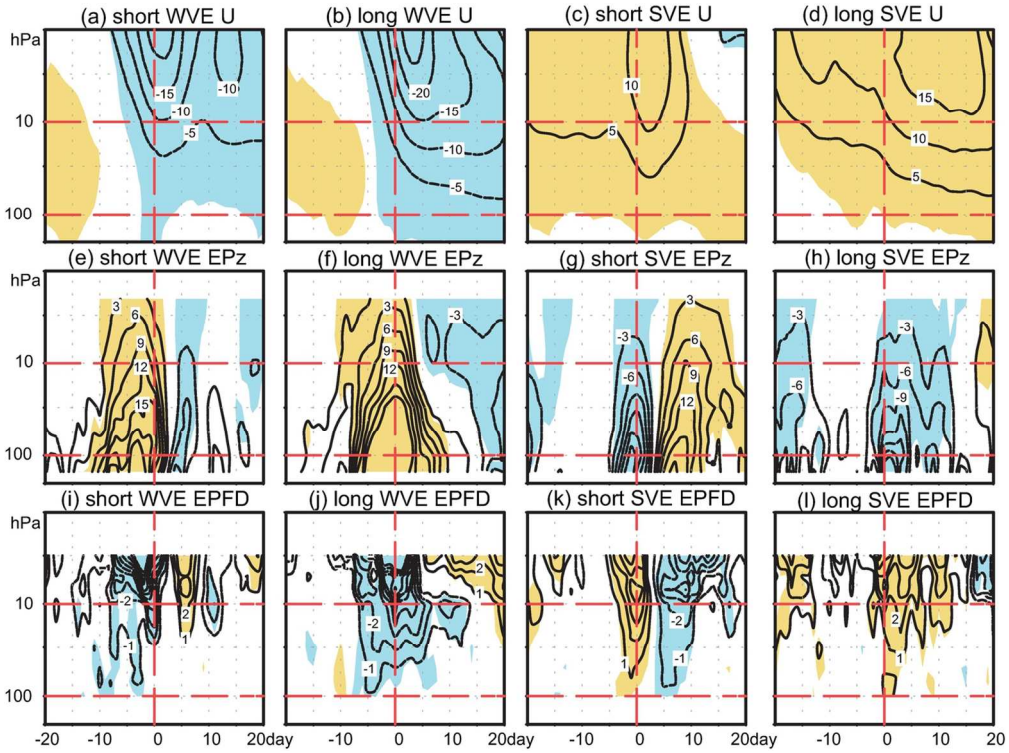

Figure 2. As in Fig. 1, but with time axis is relative to the initial day (day 0), as indicated by the vertical red line.

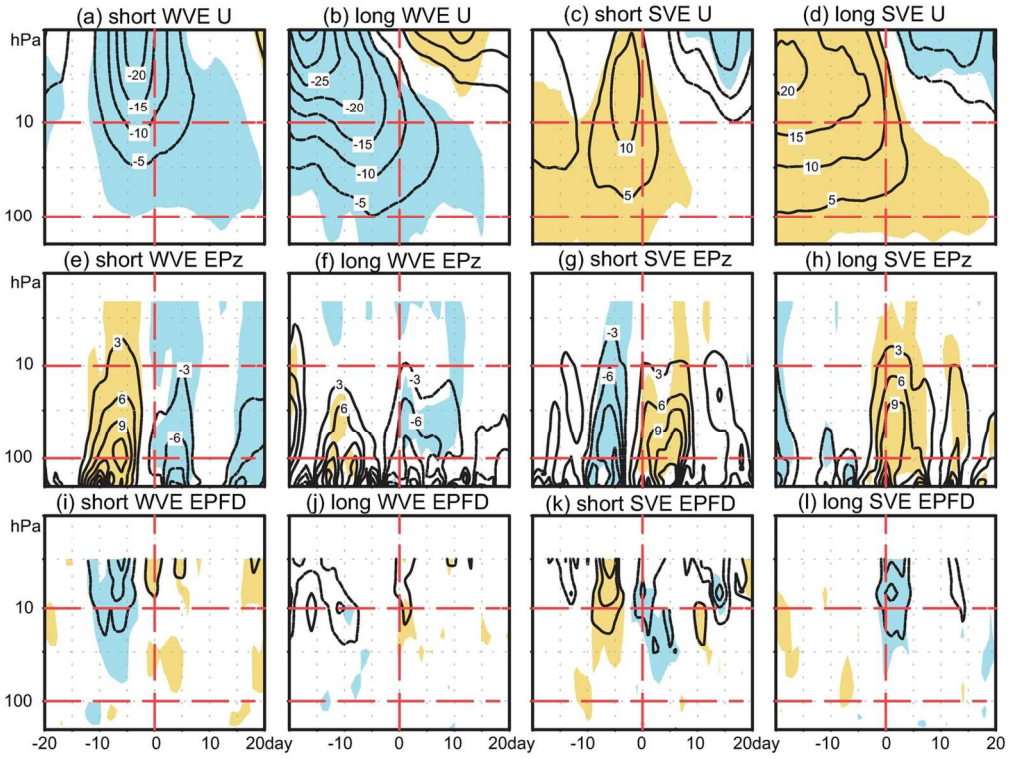

Figure 3. Composite evolution of zonal-mean zonal winds, E-P fluxes in ERA-I. As in Fig. 1, but for composite maps based on ERA-Interim reanalysis data.

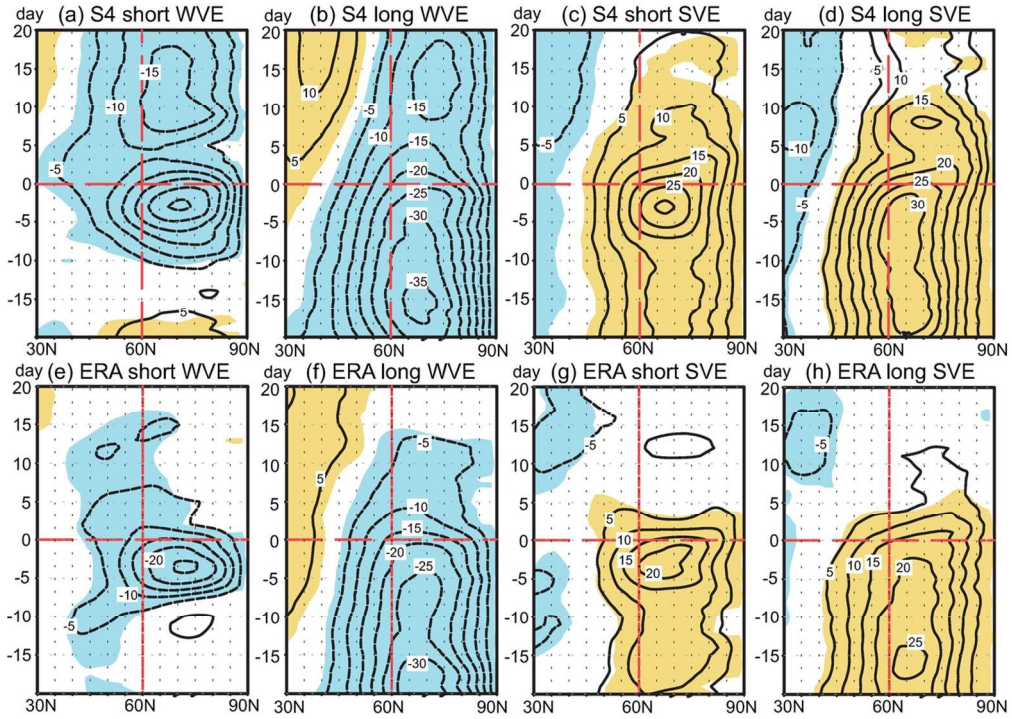

Figure 4. Composite evolution of 10-hPa zonal-mean zonal winds. (a-d) Composites of zonally-averaged anomalies in 10-hPa zonal wind with respect to the end day for short SVE, long SVE, short VWE and long VWE in S4 (contoured for every 5 m s^{-1}). (bottom row) Same as in (e-h), but for ERA-Interim reanalyses. Horizontal and vertical red lines indicate day 0 and 60N, respectively.

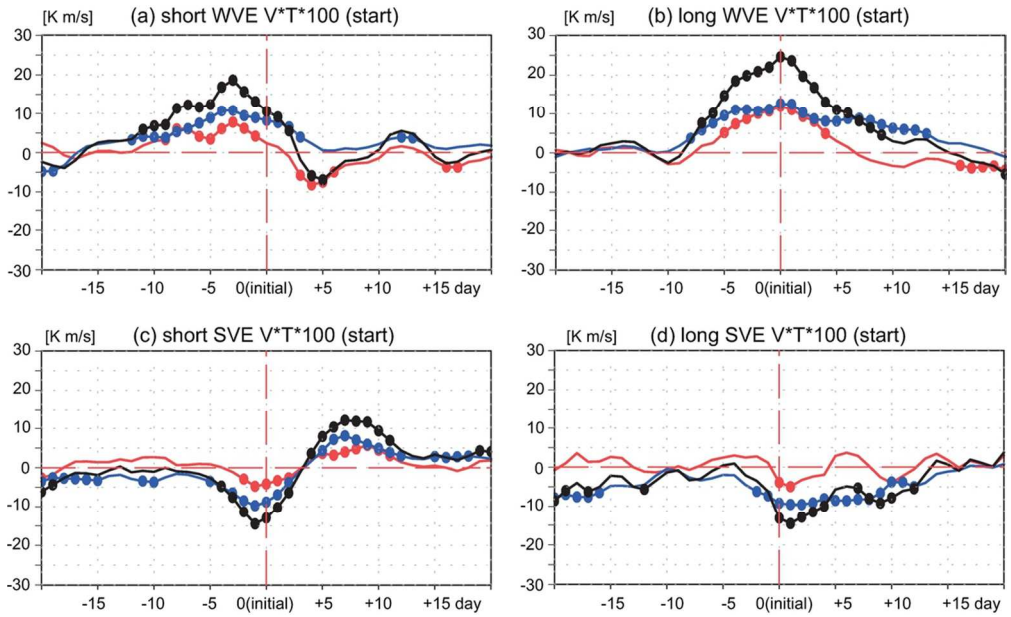

Figure 5. Time series of anomalous meridional eddy heat flux in S4. The fluxes at 100 hPa (black line: K m s^{-1}) are averaged zonally and poleward of 45N, and are based on composites constructed separately for the (a) short WVEs, (b) long WVEs, (c) short SVEs, and (d) long SVEs relative to their initial days (day 0; red dashed line). The blue and red lines represent the contributions from the quasi-linear and non-linear interaction terms, respectively, to the anomalous heat flux, with dots indicating 90% confidence level.

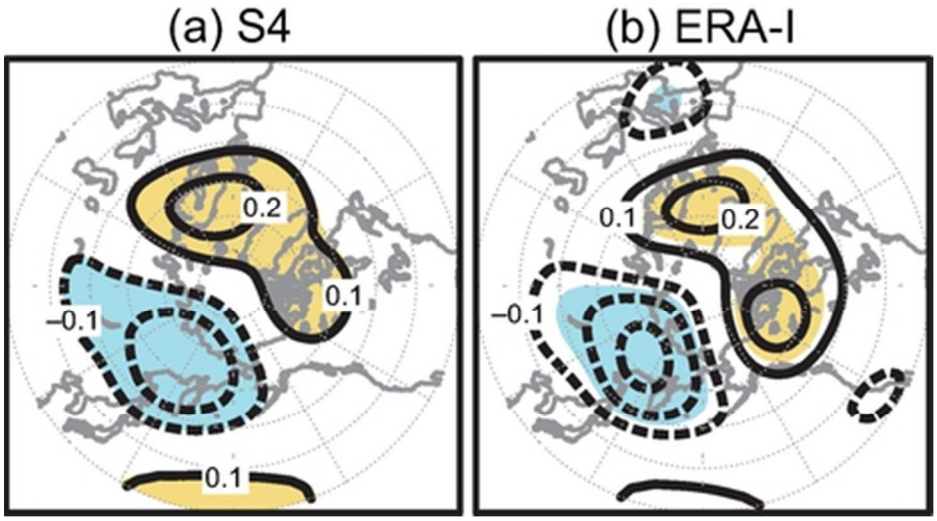

Figure 6. Correlation between 200-hPa height and 100-hPa meridional eddy heat flux anomalies in S4 and ERA-I. The correlation map between the 200-hPa height anomalies and the 100-hPa anomalous meridional eddy heat flux, averaged zonally and poleward of 45N, at a lag of – 2 days for S4 (a) and ERA-I (b), using all available days. Significant positive and negative correlations at the 99% confidence level are indicated with yellow and light blue shading, respectively.

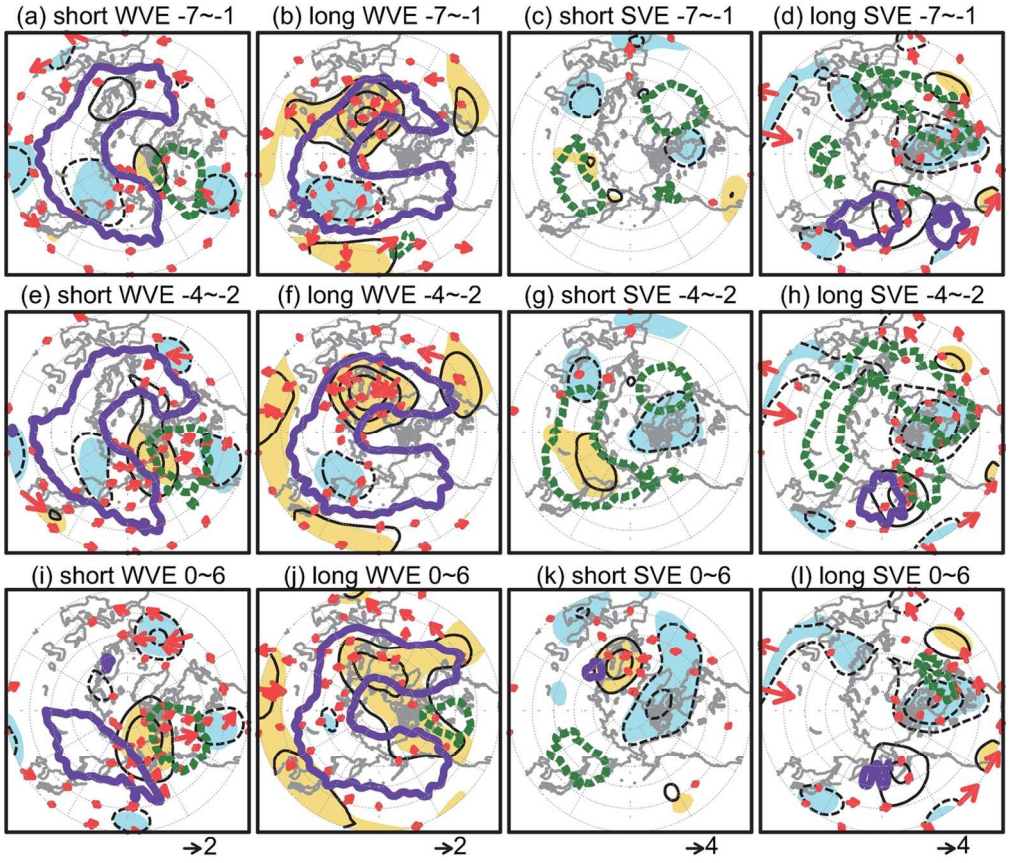

Figure 7. Composite of upper-tropospheric geopotential height anomalies in S4. Sequence of 200-hPa geopotential height composite maps (contoured for every 50 m, with solid being positive and dashed negative) for 6-day averaged periods through the life-cycle of short WVEs (first column, a-e-i), long WVEs (second column, b-f-j), short SVEs (third column, c-g-k), and long SVEs (forth column, d-h-l), centered on days [-7, -1], days [-4, 2], and days [0, 6], relative to the initial day. Significant positive and negative anomalies at the 90% confidence level are indicated with yellow and light blue shading, respectively. The purple (green) contours indicate positive (negative) 100-hPa anomalous vertical flux of wave activity (± 0.01 m^2/s^2), while red arrows indicate the 200-hPa horizontal flux of Takaya and Nakamura [2001] (m^2/s^2).

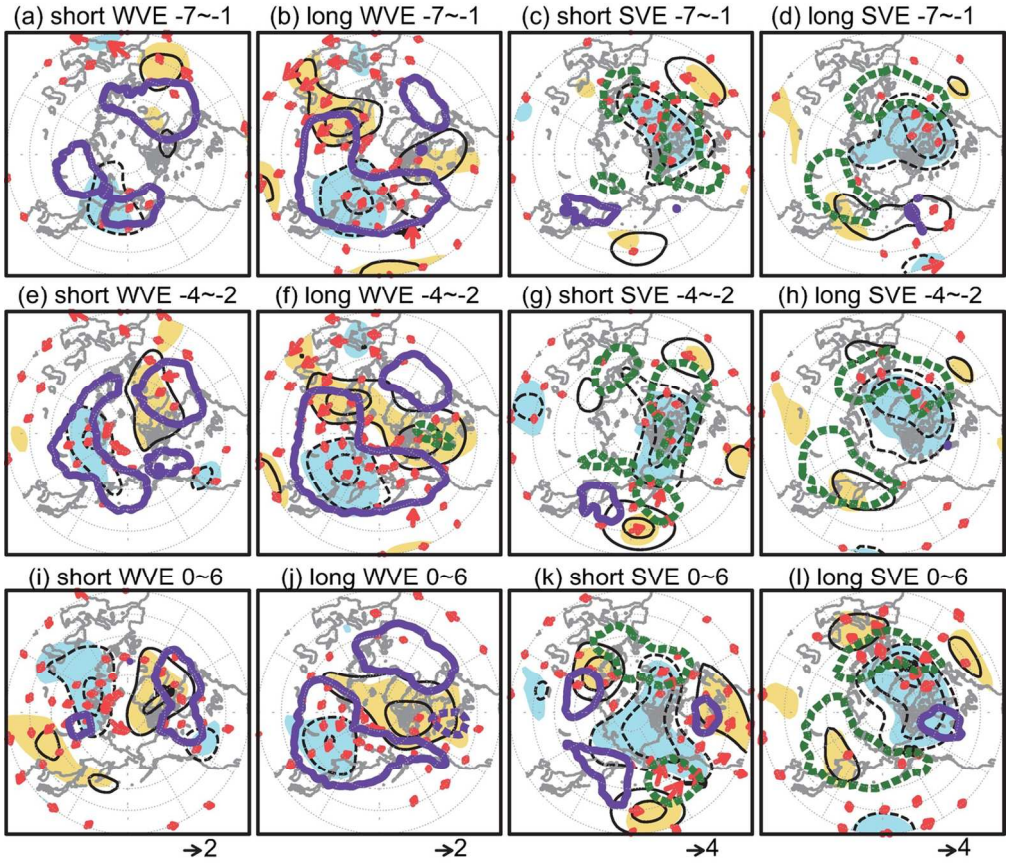

Figure 8. Composite of upper-tropospheric geopotential height anomalies in ERA-I. (As in Fig. 7).

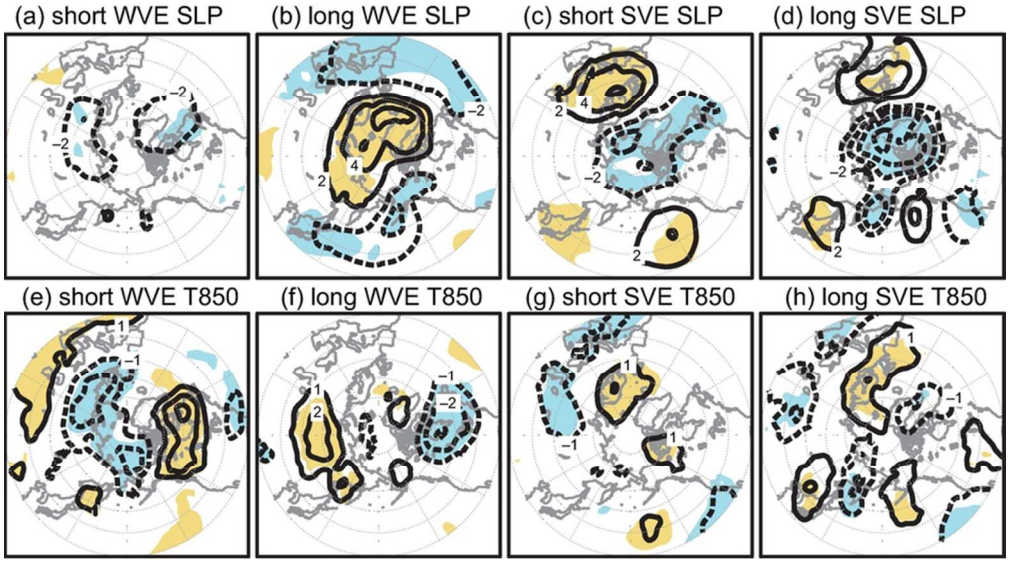

Figure 9. Composited maps of SLP and 850-hPa temperature anomalies in S4. Maps of SLP (upper; contoured for every 2 hPa) and temperature (lower; contoured for every 1 K) composited for days [1,14] with respect to the end days for short WVEs (first column, a-e), long WVEs (second column, b-f), short SVEs (third column, c-g-), and long SVEs (fourth column, d-h). Significant positive and negative anomalies at the 90% confidence level are indicated with yellow and light blue shading, respectively.

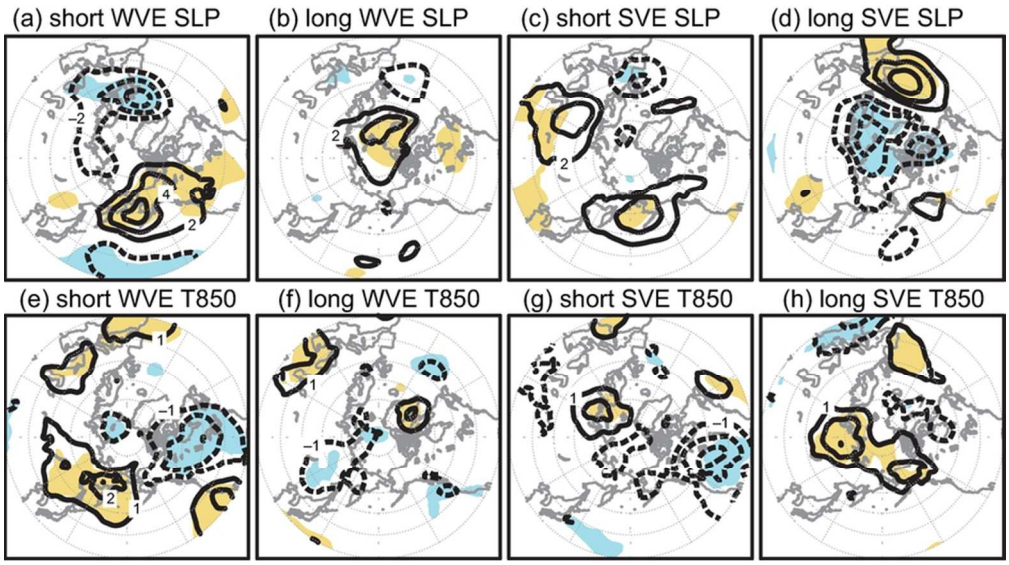

Figure 10. Composited maps of SLP and 850-hPa temperature anomalies anomalies in ERA-I. (As in Fig. 9)